PAPER

Check for updates

In situ growth of carbon dots on TiO₂ nanotube arrays for PEC enzyme biosensors with visible light response†

Cheng He,[a] Linkai Peng,[a] Linzhe Lv,[a] Yang Cao,[ab] Jinchun Tu, [iD][a] Wei Huang [iD]*[a] and Kexi Zhang*[a]

Carbon dots (CDs) were grown in situ on secondary anodized TiO₂ nanotube arrays (TiO₂ NTAs) via a hydrothermal method. The combination of CDs and TiO₂ NTAs enhanced the photoelectrochemical performance. Morphology, structure, and elemental composition of the CDs were characterized. No simple physical adsorption was found between the CDs and TiO₂, but chemical bonds were formed. UV-vis absorption and fluorescence spectroscopy showed that the CDs could enhance the absorption of TiO₂ in the visible and near-infrared regions. Owing to their up-conversion fluorescence properties, the CDs could convert low-energy photon absorption into high-energy photons, which may be used to excite TiO₂ to produce a stronger photoelectric response. Moreover, the CDs could effectively transport electrons and accept holes, thus contributing to the effective separation of electrons and holes during photoexcitation. Finally, the PEC biosensor was prepared by immobilizing glucose oxidase (GOx) on the surface of the composite. The PEC biosensor exhibited a broad range of 0.1–18 mM with a detection limit of 0.027 mM under visible irradiation because the composite material reflected strong light absorption for visible light, good conductivity, and good biocompatibility.

1. Introduction

Photoelectrochemical (PEC) sensing is a new chemical biomolecular analysis method.[1–3] The excitation and detection signals of a PEC sensor are light and electricity,[4] respectively. Hence, this device has a high signal-to-noise ratio and has attracted interest in biology,[5] medicine,[6] and environmental monitoring.[7]

The application of nanomaterials in PEC sensors has received extensive attention. Given that the high-energy photons of ultraviolet light could destroy biological systems, visible light is suitable to use as an excitation source in PEC sensing. However, common photocatalytic materials, such as TiO₂, mainly absorb in the ultraviolet region, and the rapid recombination of electron–hole pairs is unsatisfactory;[8,9] these phenomena limit their application in PEC biosensors.[10] Other nanomaterials such as metal nanomaterials,[11] semiconductor quantum dots,[12] and some carbon-based materials[13] have been introduced into PEC biosensors to improve photocatalysis and electrochemical activity.

Carbon dots (CDs) are carbon nanomaterials with a size of less than 10 nm (ref. 14–16) and have many excellent properties, such as wide optical absorption, strong photoluminescence (PL) emission, good chemical stability, non-toxicity, excellent biocompatibility, easy large-scale synthesis, and low cost. In particular, some CDs exhibit up-conversion fluorescence properties that could convert low-energy photons into high-energy photon emission through two- or multi-photon absorption,[17–19] CDs also have fine electrical conductivity and could efficiently transport electrons and holes. The combination of CDs and TiO₂ enhances the absorption of TiO₂ in the visible region and effectively separates photogenerated electron–hole pairs. At present, many studies were conducted on the application of CDs and TiO₂ in the field of photocatalysis.[20,21] For example, Pan et al.[22] used a composite of CDs synthesized through the hydrothermal synthesis of sucrose and TiO₂ nanotubes for RhB photo-degradation. Zhang et al.[23] combined the CDs obtained via electroplating graphite rods with TiO₂ NTAs for photocatalytic hydrogen production under visible light. Li et al.[24] used alkali-assisted electrolysis of graphite rods to obtain CDs for the selective oxidation of benzyl alcohol to benzaldehyde under near-infrared photocatalysis. However, few reports were found on the direct use of CDs/TiO₂ as a visible light-sensitive material for the synthesis of photoelectrochemical biosensors.

Enzyme activity is a key to enzyme-based biosensors. CDs contain many hydroxyl, carboxyl, and amino groups that could improve the biocompatibility of the electrode material. After the enzyme is loaded, its activity could be efficiently maintained.

Here, we aim to improve the photoelectric response of TiO₂ NTAs by sensitizing CDs and successfully applying them to the

[a]State Key Laboratory of Marine Resource Utilization in South China Sea, Key Laboratory of Tropical Biological Resources of Ministry of Education Hainan University, Haikou 570228, P. R. China. E-mail: hw_hnu@aliyun.com; zhangkexi@hainu.edu.cn

[b]Qiongtai Normal University, Haikou 570228, P. R. China

† Electronic supplementary information (ESI) available. See DOI: 10.1039/c9ra01045a

construction of a PEC biosensor after glucose oxidase (GOx) was loaded. TiO_2 NTAs generated through secondary anodization exhibited a high specific surface area and could accommodate a large number of CDs and biomolecules. The CDs were fabricated *in situ* on the surface of the semiconductor material, and the interfaces between the two were chemically bonded to enhance the stability of the composite while maintaining similar photoactivity. CDs contained a large amount of hydroxyl, carboxyl and amino groups, which could improve the biocompatibility of TiO_2 NTAs and help maintain the catalytic activity of the enzyme during the reaction. In addition, the CDs enhanced the absorption of TiO_2 in the visible region. Owing to the up-conversion fluorescence properties of the CDs, the composite enhanced the photoelectric response of TiO_2 in the visible region. The PEC biosensor could avoid the damage of biological enzyme by ultraviolet light under the excitation of visible light. Therefore, the glucose biosensor exhibited reliable detection performance for glucose under visible light irradiation.

2.   Experimental section

2.1   Materials and reagents

Titanium foils (99.6% purity) were obtained from Outhwaite New Energy Company. GOx was purchased from Shanghai Bioengineering Co. Ltd. Citric acid ($C_6H_8O_7$), 2-aminoethanol (C_2H_7NO), glucose ($C_6H_{12}O_6$), and other common reagents were acquired from Guangzhou Chemical Reagent Factory. All chemicals were of analytical grade and used without further purification. In addition, 0.1 M phosphate buffered saline (PBS; pH 7.4) was used as a supporting electrolyte throughout the experiments. All solutions were prepared in Milli-Q water.

2.2   Synthesis of TiO_2 NTAs

TiO_2 NTAs were prepared through anodic oxidation. The titanium foil (10 mm × 20 mm) was soaked in a mixture of hydrofluoric acid and nitric acid for 20 min ($HF/HNO_3/H_2O$ = 1 : 4 : 5 in volume), purified through orderly ultrasonic cleaning in ethanol and deionized water, and finally dried in air at room temperature. Anodization was conducted in a conventional two-electrode system containing 0.5 g of NH_4F, 6 mL of deionized water, and 84 mL of ethylene glycol. In this system, Ti foil was used as the anode, whereas Pt foil was used as the cathode. For the first step, the Ti foil was anodized at 60 V for 0.5 h, and the grown nanotubes were then ultrasonically removed in water. The produced Ti foil was subsequently anodized at 20 V for 1 h to produce an ordered nanostructure. The samples were then washed with ethanol. The as-prepared TiO_2 NTAs were annealed at 400 °C for 3 h in Muffle furnace with a heating rate of 2 °C.

2.3   Synthesis of CDs/TiO_2 NTAs

The synthesis process of CDs/TiO_2 NTAs is shown in Scheme 1. Citric acid (2.1 g) and ethanolamine (1.8 mL) were dissolved in 10 mL of deionized water and stirred vigorously for 10 min. The reaction solution was then transferred to 30 mL Teflon autoclave, added with TiO_2 NTAs, and then maintained at 180 °C for

8 h. The obtained titanium sheet was washed with ultrapure water to remove the non-adsorbed CDs and then air-dried at room temperature.

2.4   Fabrication of GOx-CDs/TiO_2 NTAs

In brief, 10 μL of glucose oxidase solution and 10 μL of chitosan solution were gradually added to the surface of CDs/TiO_2 NTAs, which were then dried at 4 °C for further use.

2.5   Characterizations

Field emission scanning electron microscope (FESEM) images were recorded using Hitachi SU8010, and transmission electron microscopy (TEM) images were recorded using JEOL JEM 2100. X-ray diffraction (XRD) was conducted on D8 Tools XRD. Fourier transform infrared spectra (FTIR) were measured by TENSOR27 FTIR spectrometer. X-ray photoelectron spectra (XPS) were recorded using Thermo Scientific ESCALAB250 with Al radiation. Raman scattering spectra (Raman) were obtained using inVia Reflex confocal Raman microscope. The UV-visible absorption spectrum and photoluminescence spectrum (PL) were measured by and Hitachi F-7000, respectively.

2.6   Photoelectrochemical measurements

Photoelectrochemical measurements were performed in a three electro cell with GOx-CDs/TiO_2 as the working electrode, platinum as the counter electrode, and Ag/AgCl as the reference electrode. Photocurrent measurements were conducted with a CHI660A electrochemical workstation. A 500 W Xenon lamp with a 380 nm cutoff filter was used as the light source. In addition, 0.1 M PBS (pH 7.4) was used as the electrolyte with a volume of 50 mL in an electrochemical cell, and 10 μL of liquid with different glucose concentration was injected. The time-dependent photocurrent switch was performed in PBS containing 0.5 mM glucose under repeated on/off visible light illumination.

3.   Results and discussion

3.1   Characterizations of CDs, TiO_2 NTAs, and CDs/TiO_2 NTAs

The structural and morphological properties of CDs and CDs/TiO_2 NTAs were studied by TEM and XRD. The TEM image of CDs indicated their monodispersity (Fig. 1A). Their size was mainly between 3.5 nm and 5 nm with an average of 4 nm as shown in the inset of Fig. 1A. The high-resolution TEM image (Fig. 1B) revealed lattice spacing of approximately 2.1 Å, which corresponded with the (100) spacing of graphitic carbon.[25]

According to Fig. 1C and D, the TiO_2 NTAs possessed a uniform nanotube array structure, and the diameter of the tube was 100 nm on average. This structure is advantageous for light absorption and has sufficient space for loading CDs. The TEM image in Fig. 1D shows that TiO_2 NTAs exhibited a tubular structure. In the HRTEM image (inset of Fig. 1D), the CDs were dispersed on the surface of TiO_2 nanotubes, indicating the successful recombination of CDs and TiO_2 NTAs. The lattice spacings of 2.1 and 3.5 Å in the inset of Fig. 1D corresponded to
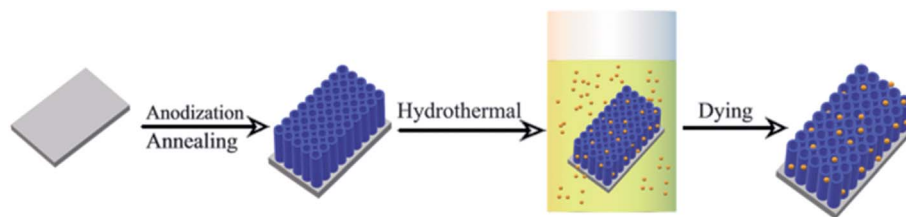
Scheme 1 Schematic illustration for the preparation of CDs/TiO$_2$.

the (100) plane of graphitic carbon in CDs and the (101) plane of anatase in TiO$_2$,[26] respectively. This finding is consistent with the lattice fringes of the CDs in Fig. 1B. As shown in Fig. S1,† the Ti and O elements distribute densely throughout the view, while the C element exhibits discretely distribution, indicating the successful loading of CDs on the TiO$_2$ TNAs.

The XRD pattern (Fig. 2A) shows that TiO$_2$ NTAs and CDs/TiO$_2$ NTAs exhibited the same characteristic diffraction peaks of anatase and Ti (JCPDS card no. 21-1272 and no. 44-1294).[27] No characteristic diffraction peak of C was detected, which may be attributed to the low content of CDs in the composite. Moreover, the synthesis of CDs did not affect the crystal structure of TiO$_2$.

The chemical composition and related chemical bonds of CDs/TiO$_2$ NTAs were studied by XPS. Fig. 2B presents the XPS full survey spectrum of the TiO$_2$ NTAs and CDs/TiO$_2$ NTAs. Carbon (C 1s), titanium (Ti 2p), oxygen (O 1s), and nitrogen (N 1s) were observed in the CDs/TiO$_2$ NTAs. The newly emerging N peak in CDs/TiO$_2$ NTAs was derived from CDs and could clearly indicate the successful combination of CDs and TiO$_2$. Ti 2p spectrum of TiO$_2$ NTAs and CDs/TiO$_2$ NTAs (Fig. 2C) exhibit the same two peaks at 458.2 and 464.1 eV, respectively, which corresponded to Ti 2p$_{3/2}$ and Ti 2p$_{1/2}$, respectively, which is assigned to Ti^{4+} 2p peaks.[28,29] The C 1s spectrum of CDs/TiO$_2$

NTAs (Fig. 2D) showed four peaks at 284.8, 285.6, 286.3, and 288.2 eV, which were attributed to C–C, C–H, C–O, and C=O, respectively. No peak of Ti–C was found in Fig. 2D, indicating that the CDs were not doped into the bulk of TiO$_2$. The N 1s spectrum of CDs/TiO$_2$ NTAs (Fig. 2E) showed three peaks at 399.7, 400.5, and 401.3 eV, which were identified as pyrrolic N, graphitic N, and amino N(N–H), respectively. The O 1s spectrum of CDs/TiO$_2$ NTAs showed four peaks at 529.8, 530.2, 531.1, and 531.8 eV. The peak at 529.8 was attributed to the oxygen in crystal lattice (Ti–O–Ti), and that at 531.8 eV was attributed to Ti–OH bonding or the existence of the hydroxyl groups (–OH) on the surface of CDs. The other two peaks at 530.2 and 531.1 eV were attributed to the C=O and Ti–O–C,[30–33] respectively. In the present case, the peak at 531.1 eV was generated by the Ti–O–C bond. These results indicated that a hybrid might have been formed in the CDs-TiO$_2$ by a Ti–O–C bond.

From the FT-IR spectra in Fig. 3A, the common absorption peaks at 3420 cm^{-1} and 1643 cm^{-1} were attributed to the stretching and bending vibrations of water absorbed on the surface of substance material, respectively. Some new peaks were observed in CDs/TiO$_2$ NTAs compared with the pure TiO$_2$ NTAs. For example, the peaks at 1560 cm^{-1} (C=O), 1392 cm^{-1} (C–O), and 1066 cm^{-1} (C–O–C) were ascribed to the addition of CDs, thereby confirming their presence in the CDs/TiO$_2$ NTAs.
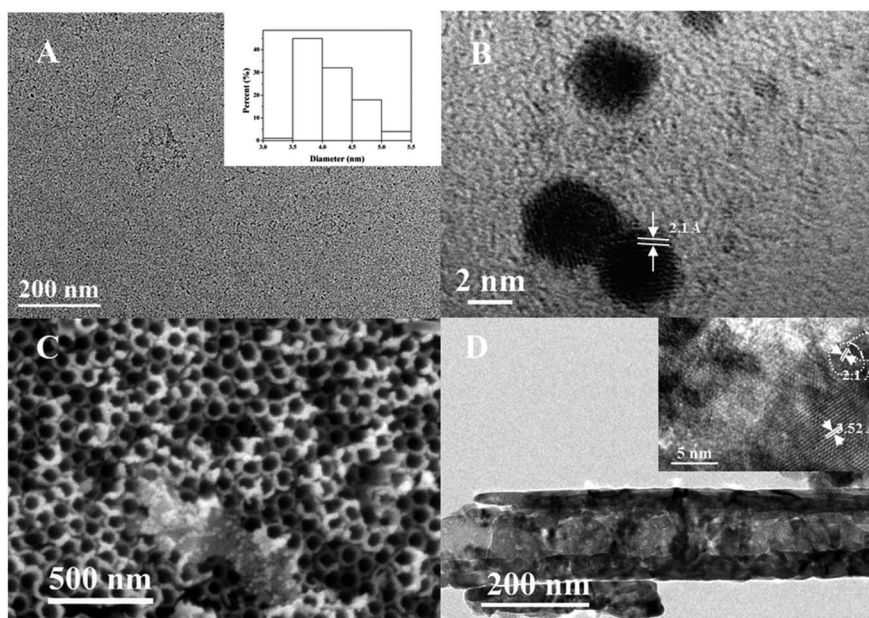

Fig. 1 (A) TEM image of the CDs, inset: size distribution histogram of CDs; (B) HRTEM of the CDs; (C) SEM of TiO$_2$ NTAs; (D) TEM of CDs/TiO$_2$ NTAs, inset: HRTEM of CDs/TiO$_2$ NTAs.
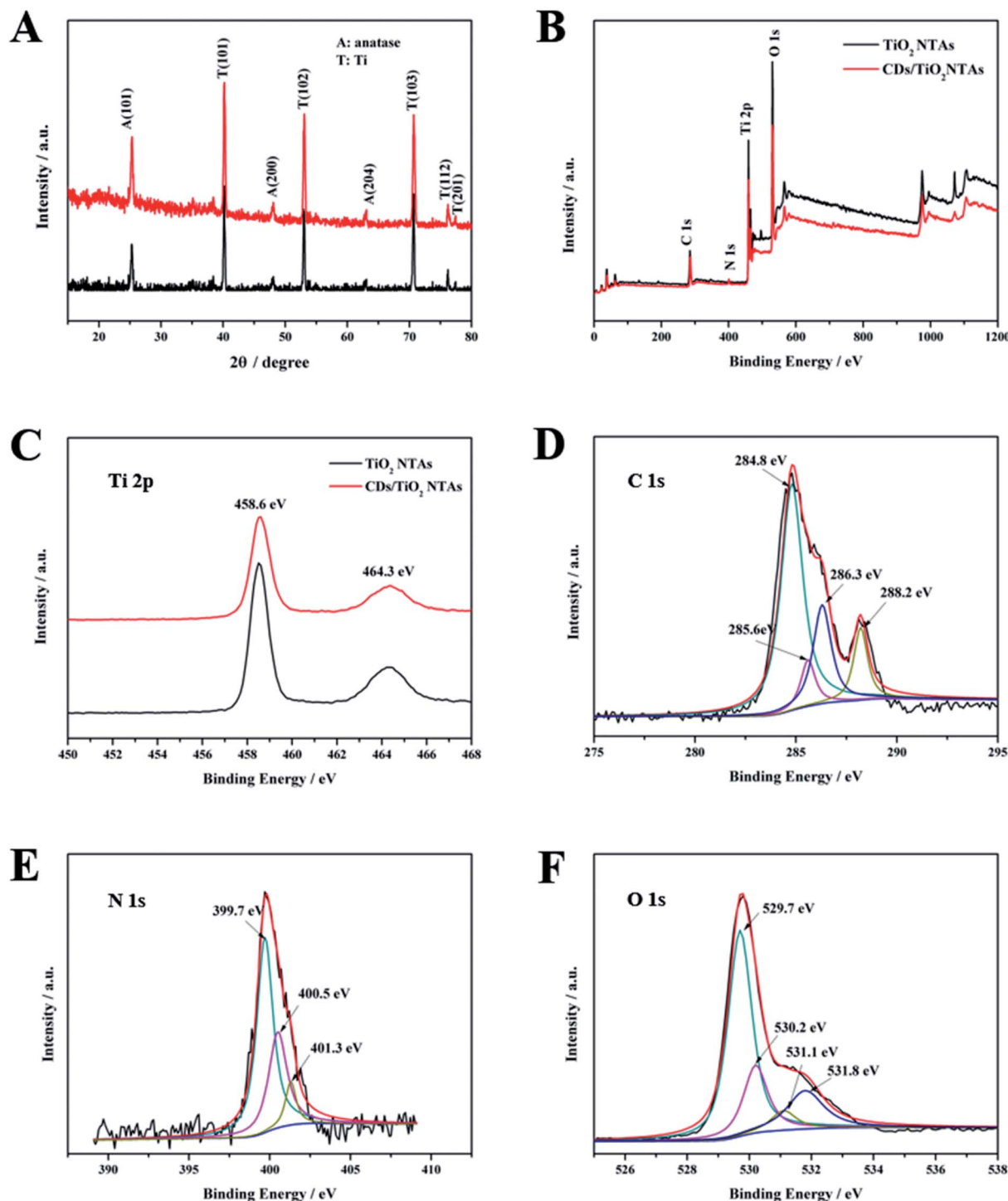
Fig. 2 (A) XRD pattern of TiO$_2$ NTAs (black line) and CDs/TiO$_2$ NTAs (red line); (B) XPS spectra of TiO$_2$ NTAs and CQDs/TiO$_2$ NTAs; (C) Ti 2p core level of TiO$_2$ NTAs and CDs/TiO$_2$ NTAs, respectively; (D–F) C 1s, N 1s, and O 1s core level spectra of CDs/TiO$_2$ NTAs, respectively.

The peak of the nitrogen-containing functional group in FTIR was not evident due to the low nitrogen content. Maintaining the activity of the enzyme is beneficial because the presence of these functional groups allows the composite to achieve good biocompatibility.

From the Raman spectra in Fig. 3B, both TiO$_2$ NTAs and CDs/TiO$_2$ NTAs exhibited four distinct characteristic peaks located near the center at 143 cm^{-1}, 393 cm^{-1}, 514 cm^{-1}, and 634 cm^{-1},

which were attributed to the Raman active modes of anatase.[34,35] In addition, CDs/TiO$_2$ NTAs showed two low intensity characteristic peaks at 1322 and 1545 cm^{-1}, which corresponded to the D and G bands of CDs, respectively. In comparison of the Raman B$_{1g}$ peaks of TiO$_2$ NTAs and CDs/TiO$_2$ NTAs, the peaks of CDs/TiO$_2$ NTAs at 397.1 and 517.2 cm^{-1} showed red shifts of 3.6 and 2.4 cm^{-1}, respectively, compared with those of TiO$_2$ NTAs. The movement of the Raman peak in the composite may be due
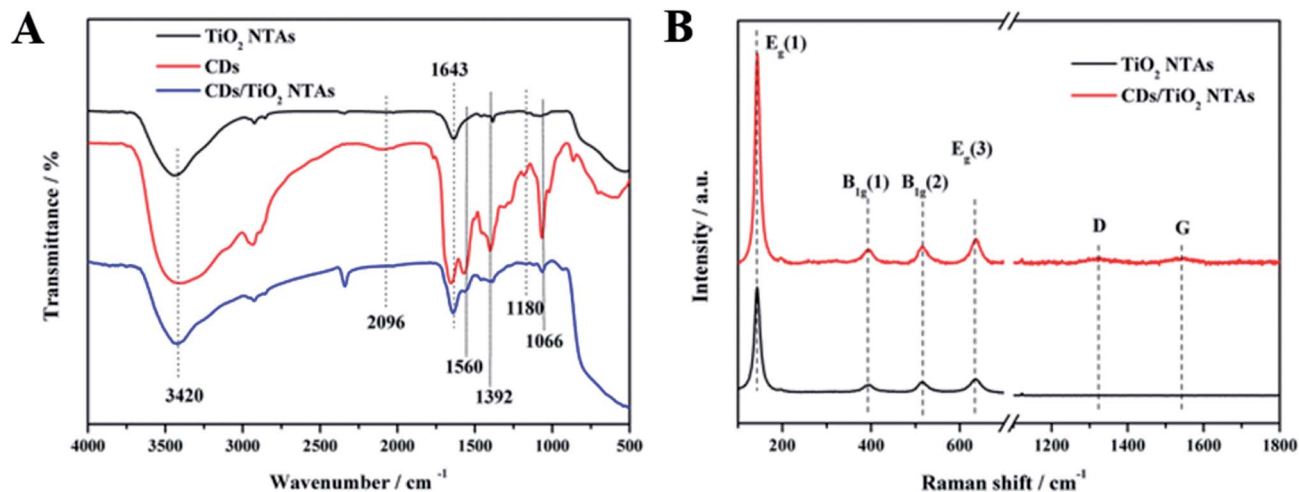
Fig. 3 (A) FTIR spectra of TiO$_2$ NTAs, CDs, and CDs/TiO$_2$ NTAs; (B) Raman spectra of TiO$_2$ NTAs and CDs/TiO$_2$ NTAs.

to the strong interaction of the formed Ti–O–C bonds.[36,37] These results indicated a strong interaction between CDs and TiO$_2$ through chemical bonding rather than through simple physical adsorption.

The results of HRTEM, XPS, and FTIR measurements indicated the successful preparation of the composite and suggested that the CDs were neither doped into the crystal phase of TiO$_2$ nor simply physical adsorbed. The CDs and TiO$_2$ were connected by chemical bonds, thereby making the composite highly conducive to electron transfer during photoelectrochemical reaction.

UV-visible absorption spectra were obtained by testing with PerkinElmer Lambda 750s. A 60 mm integrating sphere was used during the test. The test range is from 250 to 800 nm, the data interval was 1 nm and the scanning speed was 266.75 nm min^{-1}. The UV-vis absorption spectrum of TiO$_2$ NTAs (Fig. 4A) shows strong absorption in the ultraviolet region as determined by the band gap of anatase itself. The absorption at 400 nm to 800 nm was due to the inherent defects of the material. Therefore, TiO$_2$ NTAs can absorb visible and near-

infrared light. After the CDs were loaded, the absorption of TiO$_2$ NTAs in the visible region was significantly enhanced.

The UV-vis absorption spectrum of the CDs solution (Fig. 4B) shows that the two distinct absorption peaks at 244 and 337 nm corresponded to the π–π* and n–π* transitions of CDs, respectively. As observed in their up-conversion fluorescence spectrum (inset of Fig. 4B), the CDs emitted short-wavelength light (350–600 nm) under the excitation of long-wavelength light (from 550 nm to 700 nm). This up-conversion photoluminescence mechanism is due to the simultaneous absorption of two or more photons, thereby shortening the wavelength (anti-Stokes type emission) and increasing the energy of the emitted light to be higher than that of the excitation light. It is worth noting that the absorption range of TiO$_2$ in the ultraviolet region was less than 390 nm, which could be revealed from the experiments. What's more, the carbon dots could be excited by long-wavelength light through the absorption of two-photon or multi-photon. Compared with the band gap of TiO$_2$, the energy of light emitted in the range of 350–390 nm was higher so that electron/hole pairs could be emerged while TiO$_2$ was excited by
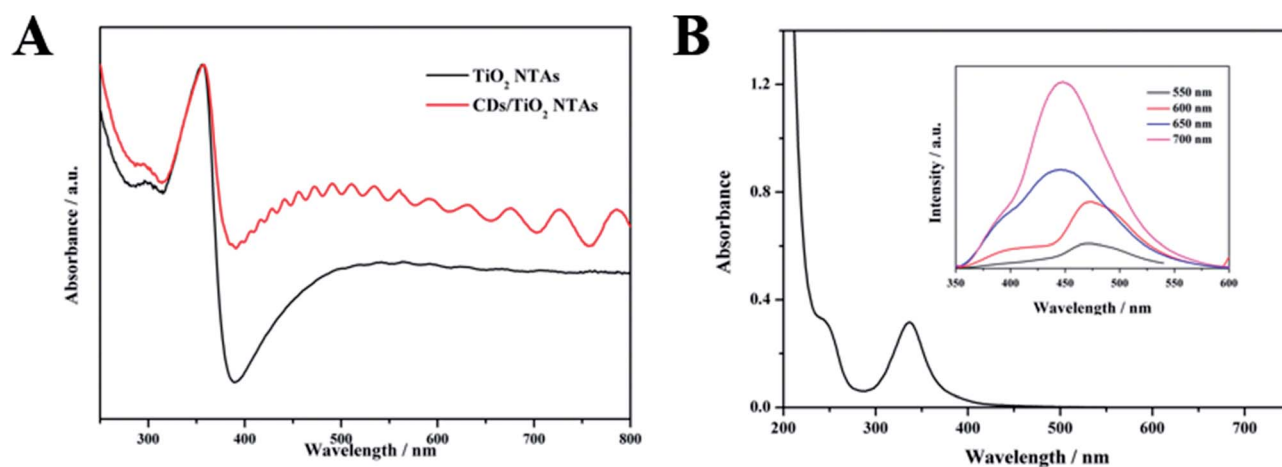

Fig. 4 (A) UV-vis absorption spectra of TiO$_2$ NTAs and CDs/TiO$_2$ NTAs; (B) UV-vis absorption spectra of CDs, inset: up-conversion fluorescence spectrum of CDs, excitation wavelengths are 550, 600, 650 and 700 nm, respectively.

means of it. Herein, the photoelectric response of TiO$_2$ could be enhanced.[38]

3.2 PEC response of the PEC biosensor assembly process

The assembly process of the sensor was evaluated through the PEC response. Fig. 5 shows the photocurrent of the electrode under visible light irradiation at a bias of 0.4 V after each modification step. The curve a in Fig. 5 reflected a small photocurrent intensity. Given that TiO$_2$ mainly absorbed ultraviolet light, its utilization of visible light was low. The photocurrent intensity of CDs/TiO$_2$ NTAs (curve b) was nearly doubled compared with that of TiO$_2$ NTAs due to the sensitization of CDs. A set of comparative experiments was conducted by immersing the anodized TiO$_2$ NTAs in the prepared CDs solution for 12 hours to obtain immersed-CDs/TiO$_2$ NTAs. Fig. 5 reveals that the photocurrent intensity of immersed-CDs/TiO$_2$ NTAs (curve c) was lower than that of CDs/TiO$_2$ NTAs, indicating that the close interfacial interaction between the hydrothermally grown *in situ* CDs and TiO$_2$ NTAs is favorable for charge transfer. When the GOx was fixed on the electrode, the photocurrent of GOx-CDs/TiO$_2$ (curve d) was slightly reduced compared with that of CDs/TiO$_2$ NTAs. Because GOx is loaded on the surface of TiO$_2$, it not only affects the absorption of light by the material itself, but also the poor conductivity of GOx, which hinders the electron transfer process.

3.3 Principle of the PEC biosensor

The GOx-CDs/TiO$_2$ electrode could increase the efficiency of electron transfer due to the chemical bond between CDs and TiO$_2$. When CDs/TiO$_2$ NTAs were irradiated with visible light, a small amount of visible light could be absorbed due to the defects on the material's surface. TiO$_2$ and CDs were simultaneously excited to generate electron–hole pairs, and the electrons of the excited state of CDs could be transferred to the conduction band of TiO$_2$. Owing to their up-conversion fluorescence properties, CDs could simultaneously absorb two or more long-wavelength photons to generate electronic

transitions, and the emitted short-wavelength light may be used to excite TiO$_2$ and further enhance the photocurrent. CDs are excellent conductors that could efficiently transport electrons and accept holes from TiO$_2$. Therefore, the generated electron–hole pairs could be effectively separated during the entire visible light excitation process. In the presence of dissolved oxygen, the GOx could catalyze the electro-oxidation of glucose to produce H$_2$O$_2$. When the electrode material was irradiated with visible light, the photogenerated electron–hole pairs were effectively separated, and H$_2$O$_2$ acted as an electron donor in combination with the photogenerated holes to generate O$_2$.[39] Throughout the process, O$_2$ acted as an effective electron transporter between the enzyme-catalyzed redox center and the sensor surface, thereby increasing the photocurrent.

Scheme 2 illustrates the reaction progress of GOx-CDs/TiO$_2$ with glucose. The FAD in the GOx, which was adsorbed on the surface of the CDs/TiO$_2$ NTAs, oxidized the glucose in the solution and became a reduced FADH$_2$. The dissolved O$_2$ then oxidized FADH$_2$ to FAD and produced H$_2$O$_2$. When the visible light irradiated the electrode material, the photogenerated holes reacted with H$_2$O$_2$ to form O$_2$, which in turn simultaneously promoted the catalytic oxidation of glucose by GOx and enhanced the photocurrent and the performance of the sensor.

3.4 PEC evaluation of the PEC biosensor

Fig. 6A shows the photocurrent *versus* time curves obtained for the GOx-CDs/TiO$_2$ NTA biosensors with glucose concentrations increasing from 0.1 mM to 18 mM. The photocurrent changes in glucose concentration are summarized in the corresponding concentration dependent calibration curves shown in Fig. 6B. The inset of Fig. 6B shows the linear correlation of the photocurrent response to the logarithm of glucose concentration from 0.1 mM to 18 mM. The regression equation was $I = 43.73 + 4.61 \log C_{glucose}$ (mM) with the correlation coefficient of 0.992. A sensitivity of 4.63 $\mu A\,mM^{-1}\,cm^{-2}$ and a detection limit (at a signal-to-noise ratio of 3) of 0.027 mM were estimated. The analytical performance of GOx-CDs/TiO$_2$ biosensor showed superiority over some previously reported PEC sensors that are tabulated in Table 1.

A time-dependent photocurrent switch of GOx-CDs/TiO$_2$ NTAs in the presence of 0.1 mM glucose was monitored under
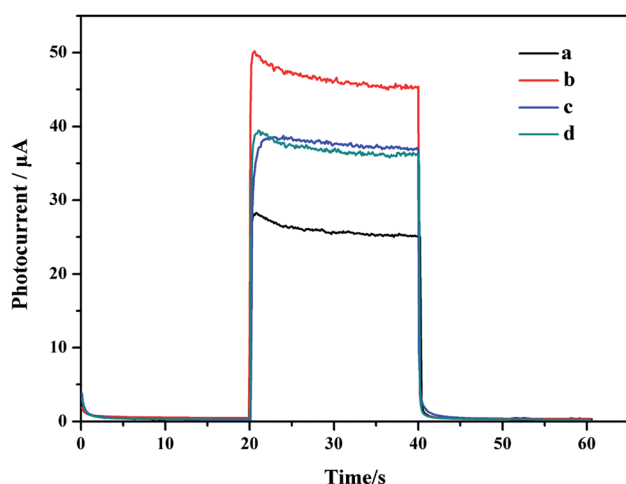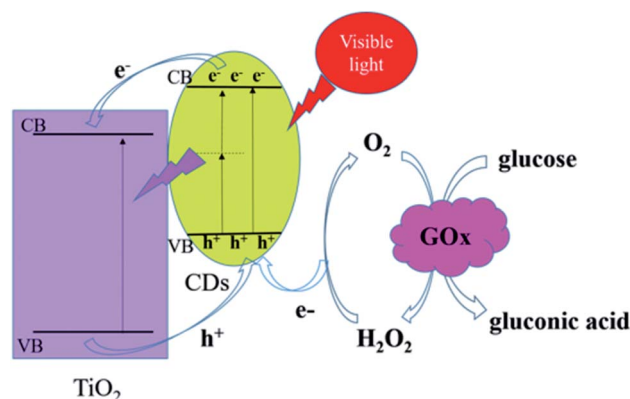

Fig. 5 Photocurrent response of TiO$_2$ NTAs (a), CDs/TiO$_2$ NTAs (b), immersed-CDs/TiO$_2$ NTAs (c), and GOx-CDs/TiO$_2$ NTAs (d).

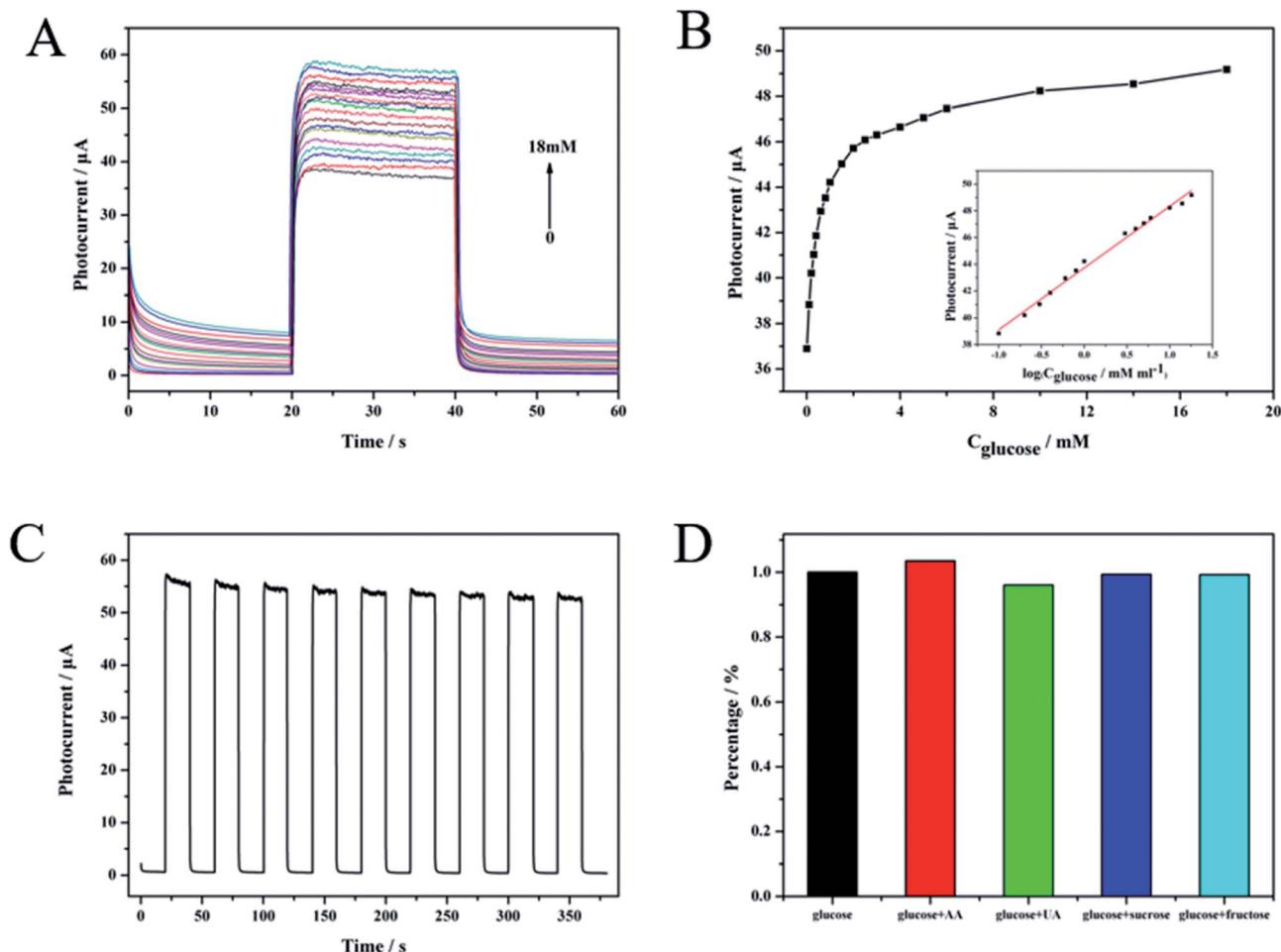**Scheme 2** Mechanism for PEC detection of glucose by GOx-CDs/TiO$_2$ NTAs.

Fig. 6 (A) Photocurrent response of GOx-CDs/TiO$_2$ at an applied potential of 0.4 V with corresponding increasing glucose concentration from 0.1 mM to 18 mM; (B) photocurrent *vs.* glucose concentration curve from 0 mM to 18 mM, inset: calibration curve for the detection of glucose with the concentration ranging from 0.1 mM to 18 mM. (C) Time-dependent photocurrent response of CDs/TiO$_2$ in the presence of 1 mM glucose under repeated on/off visible light illumination; (D) photocurrent response of GOx-CDs/TiO$_2$ in 0.1 M PBS (pH 7.4) containing 1 mM glucose and 0.1 mM other interferents: ascorbic acid (AA), uric acid (UA), fructose, and sucrose.

Table 1 Detection performance of several related GOx PEC biosensors

GOx PEC biosensors	Dynamic range/mM	Detection limit/mM	References
ITO/NiO/CdS/GOx	0.05–7.1	0.01	40
GOx|g-C$_3$N$_4$–TiO$_2$|ITO	0.05–16	0.01	41
ITO/TiO$_2$–Co$_3$O$_4$-CNT-GOx	0.5–4	0.00016	42
ITO/MoS$_2$–TiO$_2$/GOx	0.1–10	0.015	43
GOx-CDs/TiO$_2$ NTAs	0.1–18	0.027	This work

repeated on/off visible light illumination to investigate the stability of the sensor (Fig. 5E). After nine on/off cycles, the current response remained above 95% of the initial value, indicating the high stability of this sensor. The photoelectric response to biological and chemical interference (0.1 mM) of the designed PEC sensor was also compared with that of glucose (1 mM) to reveal the selectivity of the former. The photocurrent change from the interferent was less than 4% and strongly contrasted with the strong reaction of glucose (Fig. 6D). These results indicated that the GOx-CDs/TiO$_2$ NTA biosensor exhibits excellent selectivity for glucose.

4. Conclusion

CDs were grown *in situ* on second anodized TiO$_2$ NTAs by hydrothermal method to obtain CDs/TiO$_2$ NTA composites, which were then successfully applied to a PEC glucose biosensor. The successful combination of CDs and TiO$_2$ NTAs was confirmed by electron microscopy and spectroscopy. A chemical bond, not simple physical adsorption, was formed between them. According to the PEC measurement under visible light, the photoelectric response of CDs/TiO$_2$ NTAs was nearly doubled compared with that of TiO$_2$ NTAs. This ability

was derived from the excellent electron transfer capability and up-conversion fluorescence properties of CDs. The GOx-CDs/TiO₂ NTA sensor exhibited good performance in PEC detection of glucose. The PEC sensor under visible light is less damaging to biomolecules and thus shows great potential as a safe, effective, fast, and convenient glucose-detecting device.

Conflicts of interest

There are no conflicts to declare.

Acknowledgements

References

1 G. Wang, Q. Wang, W. Lu and J. Li, *J. Phys. Chem. B*, 2006, **110**, 22029–22034.

2 Z. Yue, F. Lisdat, W. J. Parak, S. G. Hickey, L. Tu, N. Sabir, D. Dorfs and N. C. Bigall, *ACS Appl. Mater. Interfaces*, 2013, **5**, 2800–2814.

3 H. Huo, Z. Xu, T. Zhang and C. Xu, *J. Mater. Chem. A*, 2015, **3**, 5882–5888.

4 W.-W. Zhao, J.-J. Xu and H.-Y. Chen, *Chem. Soc. Rev.*, 2015, **44**, 729–741.

5 X. Du, D. Jiang, L. Dai, L. Zhou, N. Hao, J. Qian, B. Qiu and K. Wang, *Biosens. Bioelectron.*, 2016, **81**, 242–248.

6 J. Sun, Y. Zhu, X. Yang and C. Li, *Particuology*, 2009, **7**, 347–352.

7 H. Li, J. Li, Z. Yang, Q. Xu and X. Hu, *Anal. Chem.*, 2011, **83**, 5290–5295.

8 B. Yan, Y. Zhuang, Y. Jiang, W. Xu, Y. Chen, J. Tu, X. Wang and Q. Wu, *Appl. Surf. Sci.*, 2018, **458**, 382–388.

9 J. S. Lee, K. H. You and C. B. Park, *Adv. Mater.*, 2012, **24**, 1084–1088.

10 W.-W. Zhao, J.-J. Xu and H.-Y. Chen, *Chem. Rev.*, 2014, **114**, 7421–7441.

11 Y. An, L. Tang, X. Jiang, H. Chen, M. Yang, L. Jin, S. Zhang, C. Wang and W. Zhang, *Chem.–Eur. J.*, 2010, **16**, 14439–14446.

12 W.-W. Zhao, Z.-Y. Ma, D.-Y. Yan, J.-J. Xu and H.-Y. Chen, *Anal. Chem.*, 2012, **84**, 10518–10521.

13 K. Wang, J. Wu, Q. Liu, Y. Jin, J. Yan and J. Cai, *Anal. Chim. Acta*, 2012, **745**, 131–136.

14 S. Y. Lim, W. Shen and Z. Gao, *Chem. Soc. Rev.*, 2015, **44**, 362–381.

15 X. T. Zheng, A. Ananthanarayanan, K. Q. Luo and P. Chen, *Small*, 2015, **11**, 1620–1636.

16 Z. L. Wu, Z. X. Liu and Y. H. Yuan, *J. Mater. Chem. B*, 2017, **5**, 3794–3809.

17 A. Salinas-Castillo, M. Ariza-Avidad, C. Pritz, M. Camprubi-Robles, B. Fernandez, M. J. Ruedas-Rama, A. Megia-Fernandez, A. Lapresta-Fernandez, F. Santoyo-Gonzalez, A. Schrott-Fischer and L. F. Capitan-Vallvey, *Chem. Commun.*, 2013, **49**, 1103–1105.

18 X. Jia, J. Li and E. Wang, *Nanoscale*, 2012, **4**, 5572–5575.

19 J. Shen, Y. Zhu, C. Chen, X. Yang and C. Li, *Chem. Commun.*, 2011, **47**, 2580–2582.

20 H. Yu, R. Shi, Y. Zhao, G. I. Waterhouse, L. Z. Wu, C. H. Tung and T. Zhang, *Adv. Mater.*, 2016, **28**, 9454–9477.

21 G. A. M. Hutton, B. C. M. Martindale and E. Reisner, *Chem. Soc. Rev.*, 2017, **46**, 6111–6123.

22 J. Pan, Y. Sheng, J. Zhang, J. Wei, P. Huang, X. Zhang and B. Feng, *J. Mater. Chem. A*, 2014, **2**, 18082–18086.

23 X. Zhang, F. Wang, H. Huang, H. Li, X. Han, Y. Liu and Z. Kang, *Nanoscale*, 2013, **5**, 2274–2278.

24 H. Li, R. Liu, S. Lian, Y. Liu, H. Huang and Z. Kang, *Nanoscale*, 2013, **5**, 3289–3297.

25 S. Qu, D. Zhou, D. Li, W. Ji, P. Jing, D. Han, L. Liu, H. Zeng and D. Shen, *Adv. Mater.*, 2016, **28**, 3516–3521.

26 J. Su, L. Zhu and G. Chen, *Appl. Catal., B*, 2016, **186**, 127–135.

27 M. Sun, X. Ma, X. Chen, Y. Sun, X. Cui and Y. Lin, *RSC Adv.*, 2014, **4**, 1120–1127.

28 Y. Yang, G. Liu, J. T. Irvine and H. M. Cheng, *Adv. Mater.*, 2016, **28**, 5850–5856.

29 Q. Wang, J. Huang, H. Sun, K.-Q. Zhang and Y. Lai, *Nanoscale*, 2017, **9**, 16046–16058.

30 M. Xing, F. Shen, B. Qiu and J. Zhang, *Sci. Rep.*, 2014, **4**, 6341.

31 R. Bangle, R. N. Sampaio, L. Troian-Gautier and G. J. Meyer, *ACS Appl. Mater. Interfaces*, 2018, **10**, 3121–3132.

32 P. Wang, S. Zhan, Y. Xia, S. Ma, Q. Zhou and Y. Li, *Appl. Catal., B*, 2017, **207**, 335–346.

33 S. Umrao, S. Abraham, F. Theil, S. Pandey, V. Ciobota, P. K. Shukla, C. J. Rupp, S. Chakraborty, R. Ahuja, J. Popp, B. Dietzek and A. Srivastava, *RSC Adv.*, 2014, **4**, 59890–59901.

34 W. F. Zhang, Y. L. He, M. S. Zhang, Z. Yin and Q. Chen, *J. Phys. D: Appl. Phys.*, 2000, **33**, 912–916.

35 T. Ohsaka, F. Izumi and Y. Fujiki, *J. Raman Spectrosc.*, 1978, **7**, 321–324.

36 G. Rajender, J. Kumar and P. K. Giri, *Appl. Catal., B*, 2018, **224**, 960–972.

37 A. C. Fernandes, L. Cunha, C. Moura, F. Vaz, P. Carvalho, E. Le Bourhis, P. Goudeau, J. P. Rivière and N. M. G. Parreira, *Surf. Coat. Technol.*, 2007, **202**, 946–951.

38 H. Zhang, H. Huang, H. Ming, H. Li, L. Zhang, Y. Liu and Z. Kang, *J. Mater. Chem.*, 2012, **22**, 10501–10506.

39 S. Wu, H. Huang, M. Shang, C. Du, Y. Wu and W. Song, *Biosens. Bioelectron.*, 2017, **92**, 646–653.

40 G. L. Wang, K. L. Liu, Y. M. Dong, X. M. Wu, Z. J. Li and C. Zhang, *Biosens. Bioelectron.*, 2014, **62**, 66–72.

41 P. Liu, X. Huo, Y. Tang, J. Xu, X. Liu and D. K. Y. Wong, *Anal. Chim. Acta*, 2017, **984**, 86–95.

42 B. Çakıroğlu and M. Özacar, *Biosens. Bioelectron.*, 2018, **119**, 34–41.

43 X. Liu, X. Huo, P. Liu, Y. Tang, J. Xu, X. Liu and Y. Zhou, *Electrochim. Acta*, 2017, **242**, 327–336.